University of Sistan and Baluchestan

Chemical Process Design

Available online at http://cpd.usb.ac.ir/

Elastic-Plastic Stress Behaviour of FGM Cylinders under Thermal and Rotational Loads: Role of Material Gradation, Temperature and Rotational Speed in Plastic Zone Propagation

Mohammad Imanparast*

Department of Mechanical Engineering, Faculty of Engineering, University of Sistan and Baluchestan, Zahedan, Iran

ARTICLE INFO

Article history:
Received: 2024-08-28
Received in revised form: 2024-11-28
Accepted: 2024-12-15
Published online: 2024-12-15

Keywords:
Elastic-plastic; Functionally graded materials; Rotating cylinder; Thermal loading, MATLAB

DOI: *10.22111/cpd.2025.51529.1052*

ABSTRACT

The primary objective of this study is to analyze the impacts of thermal loading, material composition, radius ratios, and rotational speeds on the initiation and progression of plastic zones in functionally graded cylinders. To achieve this, the problem is approached under plane strain conditions, employing Tresca's yield criterion alongside its associated flow rule to determine the onset of yielding. Two plastic regimes, dependent on stress variations with temperature, are incorporated into the analysis. A power-law distribution is applied to model the radial variations in Young's modulus, yield stress, thermal conductivity, thermal expansion coefficient, and material density. The governing equations are solved analytically across three deformation zones: elastic, elastic-plastic, and fully plastic. The resulting formulations predict the conditions for yielding initiation, considering rotational speed, temperature, material properties, and radius ratio. Numerical simulations, conducted using MATLAB, validate the analytical solutions and highlight the significant influence of thermal gradients, rotational speeds, and material characteristics on yielding behaviors. The findings suggest that altering the thermal gradient, even under constant rotational speeds and material configurations, can significantly change the location of yielding, the governing deformation regime, and the critical rotational speed necessary for plastic deformation.

1. Introduction

Materials with functionally graded properties are a type of composite characterized by gradual changes in properties in one, two, or three directions. These materials often exhibit suitable thermal and mechanical properties, enabling their wide application across various fields. In recent years, a significant amount of research has been conducted on functionally graded materials (FGMs), including elastic-plastic analyses. Below, several recent studies relevant to this topic are outlined. Extensive studies have been devoted to the investigation of rotating cylinders composed of

Corresponding author. Tel: +985431133277
E-mail address: imanparast@eng.usb.ac.ir (M. Imanparast).

homogeneous materials. A considerable number of these studies are referenced in the work of Gramer and Lence [1], where the stress distribution within the elastic and plastic regions of a homogeneous rotating cylinder was analyzed. Furthermore, Mak [2] examined the problem of a homogeneous rotating shaft under elastic and plastic conditions with a focus on plane stress. Two plastic regimes were considered based on stress values, and stress distribution, displacement, and the critical rotational velocity were determined.

Arsalan [3] analytically investigated the elastic-plastic behavior of rotating shafts with closed and open ends, considering linear work-hardening and Tresca's criterion. In another study, Arsalan [4] examined the elastic-plastic stress distribution in solid and hollow rotating shafts using the Von Mises criterion and a nonlinear work-hardening model, employing numerical methods to solve the problem. Arsalan and Mak [5] proposed a computational method to limit angular velocity to prevent secondary plastic deformation in rotating shafts with nonlinear strain hardening. This model is based on the Von Mises criterion and the J2 deformation theory.

Arsalan and Ekis [6] analyzed the elastic-plastic behavior of a long functionally graded cylinder subjected to internal pressure. In this study, they considered an ideal elastic-plastic material behavior, where only Young's modulus was treated as a parabolic function of thickness. Ekis and Arsalan [7] presented an analytical investigation of elastic-plastic behavior in functionally graded rotating shafts and disks under the assumptions of plane stress and strain. They modeled Young's modulus as a power or parabolic function of the radius. Their findings indicated that at the center of the disk and shaft, the stresses are limited, radial and tangential stresses are equal, and stress changes are independent of the elastic modulus

In subsequent research, Arsalan and Ekis [8] modeled Young's modulus and yield stress as quadratic and power functions, comparing functionally graded and homogeneous cylinders under internal pressure. Their results demonstrated that material property variations significantly impact stress distribution, suggesting that appropriate material selection can reduce stress under equal pressure conditions. Arsalan and Ekis [9] extended their work by considering nonlinear variations of Young's modulus and yield stress. They compared the elastic-plastic stresses of functionally graded and homogeneous rotating cylinders, showing that stress distributions in functionally graded materials differ significantly from those in homogeneous materials. Additionally, in functionally graded materials, plastic stresses vary with the material properties, unlike in homogeneous materials. In another study, Arsalan and Ekis [10] analyzed functionally graded rotating cylinders assuming power-law variation of Young's modulus (with other properties constant) and perfect elastic-plastic behavior. By considering a range of material property variations and three plastic regimes, they demonstrated that in functionally graded materials, depending on material distribution and rotational speed, yielding could initiate from the inner radius, outer radius, or both surfaces simultaneously.

Arsalan, Arslan, and Mak [11] investigated homogeneous rotating cylinders subjected to work-hardening and a positive temperature gradient using an analytical approach. Their findings, which considered three plastic regimes, revealed a reduction in the elastic limit speed and an increase in the fully plastic rotational speed. In this material and under the specified conditions, the initiation of yielding predicted to occur at the inner surface. Darijani, Kargarnovin, and Naghdiabadi [12] provided an analytical solution for the elastic-plastic problem of thick-walled cylinders under pressure, incorporating work-hardening effects and considering the Bauschinger effect. They optimized the autofrettage thickness in their study. Ozturk and Golgic [13] analyzed a long functionally graded metallic cylinder with closed ends and constant heat generation, modeling Young's modulus, yield stress, thermal conductivity, and

linear expansion coefficient as power-law functions. They studied the effects of material property variations on stress values and compared homogeneous and functionally graded cylinders.

Pankaj [14] examined elastic-plastic stresses in homogeneous rotating cylinders under steady-state thermal conditions. His analysis utilized the concept of total strain computation and highlighted the significant impact of temperature gradients on stress distribution. Sharma and Yadav [15], employing the finite difference method, studied elastic-plastic behavior in functionally graded steel cylinders under transient thermal loads for a limited set of material conditions. Fatehi and Zamani-Nejad [16] presented an elastic solution for functionally graded rotating cylinders based on infinitesimal elasticity theory. Their findings indicated the necessity of considering density as a radial function for predicting yielding conditions, emphasizing its considerable impact on results. Zamani-Nejad and Fatehi [17] provided an analytical solution for functionally graded rotating cylindrical vessels under internal pressure without temperature variations. Their research considered various stress conditions governing yielding and examined stress distribution and residual stresses across three plastic regimes.

Based on the reviewed literature, the initiation and expansion of the plastic zone in functionally graded rotating cylinders subjected to thermal loads have received less attention. In the present article, the elastic-plastic analysis of rotating cylinders under thermal effects addressed analytically. Considering the impact of density variations on yielding conditions, as noted in previous studies, we adopt a power-law model for Young's modulus, yield stress, thermal conductivity, linear expansion coefficient, and density in the modeling of functionally graded materials. Density variations have been considered in fewer studies. The Poisson ratio is assumed constant in this study, and can be approximated using its average value along the radius based on the material's volume fraction. The equations are formulated under the assumption of plane strain, and zero boundary pressure conditions are applied to the cylinder's inner and outer surfaces. Additionally, the inner cylinder temperature is set to $T_a > 0°$, and the outer temperature to $T_b = 0°$. Tresca's criterion is employed to determine the onset of yielding, while in the plastic range, the associated flow rule **is** used with the assumption of perfect elastic-plastic behavior.

2. Problem analysis

2.1. Elastic solution

The governing equations for the problem of a rotating cylinder are equilibrium equations, which, considering the symmetry of the problem and uniform pressure and temperature along the cylinder, result in only the equation in the r-direction being effective. Using the formulation by Goodyear and Timoshenko [18], the governing equations expressed as:

$$\frac{d\sigma_r}{dr} + \frac{\sigma_r - \sigma_\theta}{r} = -\rho r \omega^2 \tag{1}$$

In Eq. (1) $\sigma_r, \sigma_\theta, \sigma_z$ represent radial, tangential, and axial stresses, respectively. ρ denotes the material density r the radius, and ω is the rotational speed of the cylinder. All stress and density values are functions of r. Using Hooke's Law, the relation between total stress and strain given as:

$$\varepsilon_r = \frac{1}{E}[\sigma_r - \nu(\sigma_\theta + \sigma_z)] + \alpha T + \varepsilon_r^p \tag{2}$$

$$\varepsilon_\theta = \frac{1}{E}\left[\sigma_\theta - \nu(\sigma_r + \sigma_z)\right] + \alpha T + \varepsilon_\theta^p \tag{3}$$

$$\varepsilon_z = \frac{1}{E}\left[\sigma_z - \nu(\sigma_\theta + \sigma_r)\right] + \alpha T + \varepsilon_z^p \tag{4}$$

In Eqs. (2) to (4), the first term represents elastic strains, the second term represents thermal strains, and the third term represents plastic strains. α is the thermal expansion coefficient, v is Poisson's ratio, and E is Young's modulus. In this problem, the strain compatibility equation considered as:

$$\frac{d\varepsilon_\theta}{\mathrm{d}r}+\frac{\varepsilon_\theta-\varepsilon_r}{r}=0 \tag{5}$$

The relationship between strains and displacements described by Eqs. (6) and (7):

$$\varepsilon_{\mathrm{r}}\left(r\right)=\frac{\mathrm{d}u}{\mathrm{d}r} \tag{6}$$

$$\varepsilon_\theta\left(r\right)=\frac{u}{r} \tag{7}$$

The mechanical properties of FG materials vary radially, and therefore, a power-law model employed to represent the engineering constants in the above equations. Accordingly, the following values substituted into Eqs. (1) to (7):

$$E\left(r\right)=\varepsilon_0 r^{n_1} \tag{8}$$

$$\alpha=\alpha_0 r^{n_2} \tag{9}$$

$$k=k_0 r^{n_3} \tag{10}$$

$$\sigma_y=\sigma_0 r^{n_4} \tag{11}$$

$$\rho=\rho_0 r^{n_5} \tag{12}$$

In this problem, $E_0=\frac{E_i}{a^{n_1}},\alpha_0=\frac{\alpha_i}{a^{n_2}},k_0=\frac{k_i}{\alpha^{n_3}},\sigma_0=\frac{\sigma_y^i}{\alpha^{n_4}},\rho_0=\frac{\rho_i}{\alpha^{n_5}}$ represent the Young's modulus, thermal coefficient, thermal conductivity, yield stress, and density, respectively. E_i , α_i , k_i , σ_y^i , ρ_i are the values of these variables at the cylinder's inner surface, obtained using the volume fraction of two materials.

The governing equation for temperature distribution (Laplace's equation) in the radial direction of the cylinder simplified as follows, assuming uniform temperature across the inner surface: (13)

$$\frac{1}{r}\frac{d}{dr}\left[rk\left(r\right)\frac{dT}{dr}\right]=0 \tag{13}$$

By solving Eq. (13) and applying boundary conditions, $\left(T\left(a\right)=T_a;T\left(b\right)=T_b\right)$ the temperature distribution obtained as:

$$T\left(r\right)=D_1 r^{-n_3}+D_2 \tag{14}$$

$$D_1=\frac{T_a-T_a}{r_i^{-n_3}-r_0^{-n_3}} \tag{15}$$

$$D_2=Ta-D_1 r_i^{-n_3} \tag{16}$$

Using σ_θ from the equilibrium equation, σ_z from the plane strain assumption ($\sigma_z=\nu\left(\sigma_r+\sigma_\theta\right)-\alpha ET$), and temperature from Eq. (14) and substituting these relations into the strain compatibility Eq. (5) yields:

$$r^2\frac{\mathrm{d}^2\sigma_r}{dr^2}+A_1 r\frac{\mathrm{d}\sigma_r}{\mathrm{d}_r}+A_2\sigma_r=A_3\omega^2 r^{n_5+2}+A_4 r^{n_1+n_2-n_3}+A_5 r^{n_1+n_2} \tag{17}$$

where the constants A_i defined as:

$$A_1=(3-n_1) \tag{18}$$

$$A_2=-n_1\left(\frac{1-2\nu}{1-\nu}\right) \tag{19}$$

$$A_3 = -\rho_0\left(n_1 - n_5 + 2 + \frac{1}{1-\nu}\right) \quad (20)$$

$$A_4 = \left(n_3 - n_2\right)\frac{E_0\alpha_0 D_1}{1-\nu} \quad 21)$$

$$A_5 = -\frac{n_2 E_0\alpha_0 D_2}{1-\nu} \quad (22)$$

The above equation (17) is a second-order differential equation, which haven homogeneous and particular solutions that expressed as:

$$\sigma_r\left(r\right) = C_1 r^{K_1} + C_2 r^{K_2} + H_1\left(r\right)$$
$$H_1\left(r\right) = B_1\omega^2 r^{n_5+2} + B_2 r^{n_1+n_2-n_3} + B_3 r^{n_1+n_2} \quad (23)$$

where:

$$K_{1,2} = \left\{\left(1-A_1\right) \pm \sqrt{\left(1-A_1\right)^2 - 4A_2}\right\}/2 \quad (24)$$

$$B_1 = A_3 / \left\{\left(n_5+2\right)\left(n_5+1\right) + A_1\left(n_5+2\right) + A_2\right\} \quad (25)$$

$$B_2 = A_4 / \left\{\left(n_1+n_2-n_3\right)\left(n_1+n_2-n_3-1\right) + A_1\left(n_1+n_2-n_3\right) + A_2\right\} \quad (26)$$

$$B_3 = A_5 / \left\{\left(n_1+n_2\right)\left(n_1+n_2-1\right) + A_1\left(n_1+n_2\right) + A_2\right\} \quad (27)$$

Using Eq. (1) and plane strain, tangential and axial stresses expressed as:

$$\sigma_\theta\left(r\right) = C_1\left(K_1+1\right)r^{K_1} + C_2\left(K_2+1\right)r^{K_2} + B_1\left(n_5+3+\rho_0\right)\times\omega^2 r^{n_5+2}\ldots \quad (28)$$
$$+ B_2\left(n_1+n_2-n_3+1\right)r^{n_1+n_2-n_3} + \mathrm{B}_3\left(n_1+n_2+1\right)r^{n_1+n_2}$$

$$\sigma_z\left(r\right) = \nu\left(C_1\left(K_1+2\right)r^{K_1} + C_2\left(K_2+2\right)r^{K_2} + B_1\left(n_5+4\right)\times\omega^2 r^{n_5+2} + [B_2(n_1+n_2-n_3+2)\ldots.\right. \quad (29)$$
$$\left.-E_0\alpha_0 D_1/\upsilon)\right]\times r^{n_1-n_2-n_3} + [B_3\left(n_1+n_2+2\right) - E_0\alpha_0 D_2/\upsilon]\times r^{n_1+n_2}$$

Constants C1 and C2 are determined using boundary pressure conditions $\sigma_r\left(b\right) = -P_b = 0$ and $\sigma_r\left(a\right) = -P_a = 0$. Consequently:

$$C_1 = \frac{\left[\left(P_a + H_1\left(a\right)\right)\left(b/a\right)^{K_2} - \left(P_b + H_1\left(b\right)\right)\right]}{\left[b^{K_1} - a^{K_1}\left(b/a\right)^{K_2}\right]} \quad (30)$$

$$C_2 = \frac{\left[\left(P_a + H_1\left(a\right)\left(b/a\right)^{K_1}\right) - \left(P_b + H_1\left(b\right)\right)\right]}{\left[b^{K_2} - a^{K_2}\left(b/a\right)^{K_1}\right]} \quad (31)$$

2.2. Yield criterion

Based on the Tresca criterion, yielding occurs when the maximum shear stress in the material equals the maximum shear stress at the yield condition under tension. Accordingly, the yield relationship written as:

$$\sigma_y = \left|\sigma_{max} - \sigma_{min}\right| = \sigma_o r^{n_4} \quad (32)$$

In the present problem σ_{max} denotes the tangential stress, σ_{min} and represents either radial or axial stress depending on the conditions. Consequently, the function φ defined as follows to indicate the initiation of yielding:

$$\varphi_1 = \left(\left|\sigma_\theta - \sigma_r\right| - \sigma_0 r^{n_4}\right) \quad (33)$$

$$\varphi_2 = \left(\left|\sigma_\theta - \sigma_z\right| - \sigma_0 r^{n_4}\right) \quad (34)$$

2.3 Plastic region type I

In many boundary conditions governing cylindrical problems, the stress state typically follows, $\sigma_\theta > \sigma_z > \sigma_r$, and the Tresca equation reduces to $\sigma_\theta - \sigma_r = \sigma_y = \sigma_o r^{n_4}$ In this case, based on the plastic flow rule, $\varepsilon_z^P = 0$, and under the assumption of incompressibility $\varepsilon_r^P + \varepsilon_\theta^P + \varepsilon_z^p = 0$ [19]. Thus, $\varepsilon_r^P = -\varepsilon_\theta^P$ and by using Eq. (1) and Eq. (32), stress values in the plastic region can be determined as follows:

$$\sigma_r(r) = \frac{-\rho_o \omega^2 r^{n_5+2}}{n_5+2} + \frac{\sigma_o}{n_4} r^{n_4} + C_3 \tag{35}$$

$$\sigma_\theta(r) = \frac{\rho_o \omega^2 r^{n_5+2}}{n_5+2} + \frac{\sigma_o r^{n_4}}{n_4}(1+n_4) + C_3 \tag{36}$$

$$\sigma_z(r) = \frac{-2\nu\rho_o \omega^2 r^{n_5+2}}{(n_5+2)} + \frac{\nu\sigma_o r^{n_4}(2+n_4)}{n_4} + 2\nu C_3 - \alpha_o E_o D_1 r^{n_1+n_2-n_3} - \alpha_o E_o D_2 r^{n_1+n_2} \tag{37}$$

The constant C_3 in these equations depends on boundary conditions influenced by the location of yielding initiation. To compute displacements and residual strains, using the flow rule, incompressibility, and plane strain assumptions:

$$\varepsilon_r^{total} + \varepsilon_\theta^{total} + \varepsilon_z^{total} = \underbrace{\varepsilon_r^P + \varepsilon_\theta^P + \varepsilon_z^P}_{\text{compressibility=0}} + \varepsilon_r^e + \varepsilon_\theta^e + \underbrace{\varepsilon_z^e}_{=0} + 3\alpha T \tag{38}$$

From the plane strain assumption, $\varepsilon_z^{total} = 0$. According to the flow rule $\varepsilon_Z^p = 0$ and $\varepsilon_Z^e = 0$, therefore Consequently, $\sigma_z = \nu(\varepsilon_r + \varepsilon_\theta) - \alpha\ ET$ using relations (7) and (6), we have:

$$\frac{du}{dr} + \frac{u}{r} = \frac{(1-2\nu)(1+\nu)}{E(r)}(\sigma_r + \sigma_\theta) + 2(1+\nu)\alpha T \tag{39}$$

By applying the yielding condition (32), the differential equation for displacement takes the form:

$$\frac{du}{dr} + \frac{u}{r} = S_1 r^{-n_1+n_5+2} + S_2 r^{n_4-n_1} + S_3 r^{n_2-n_3} + S_4 r^{n_2} + S_5 r^{-n_1} \tag{40}$$

where,

$$S_1 = \frac{-2(1-2\nu)(1+\nu)\rho_o \omega^2}{E_o(n_5+2)} \tag{41}$$

$$S_2 = \frac{2(1-2\nu)(1+\nu)\sigma_o}{E_o n_4}\left(1 + \frac{n_4}{2}\right) \tag{42}$$

$$S_3 = 2(1+\nu)\alpha_o D_1 \tag{43}$$

$$S_4 = 2(1+\nu)\alpha_o D_2 \tag{44}$$

$$S_5 = \frac{2(1-2\nu)(1+\nu)}{E_o} C_3 \tag{45}$$

The solution for displacement is expressed as in equation:

$$u(r) = R_1 r^{n_5-n_1+3} + R_2 r^{n_4-n_1+1} + R_3 r^{n_2-n_3+1} + R_4 r^{-n_2+1} + R_5 r^{-n_1+1} + \frac{C_4}{r} \tag{46}$$

C_4 is a constant determined by boundary conditions, and the remaining terms are defined as follows:

$$R_1 = \frac{S_1}{n_5 - n_1 + 4} \tag{47}$$

$$R_2 = \frac{S_2}{n_4 - n_1 + 2} \tag{48}$$

$$R_3 = \frac{S_3}{n_2 - n_3 + 2} \tag{49}$$

$$R_4 = \frac{S_4}{2 - n_2} \tag{50}$$

$$R_5 = \frac{S_5}{2 - n_1} \tag{51}$$

The total tangential strain and displacement are given by $\varepsilon_\theta^{total} = u / r$, which can be expressed as $\varepsilon_\theta^P = -\varepsilon_r^P = \varepsilon_\theta^{total} - \varepsilon_\theta^e - \alpha T$ Using the yielding condition and elastic strain relations:

$$\varepsilon_\theta^e(r) = \frac{1}{E}\left(\left(1-\nu-\nu^2\right)\left[\frac{-\rho_o \omega^2 r^{n_5+2}}{n_5+2} + \frac{\sigma_o}{n_4} r^{n_4} + C_3\right] + \left(1-\nu^2\right)\sigma_o r^{n_4}\right) \tag{52}$$

Therefore, by utilizing Eq. (52) and substituting it into the $\varepsilon_\theta^{total}$ relationship for, the value of ε_θ^P can be determined. Additionally, using $\varepsilon_r^P = -\varepsilon_\theta^P$, the radial plastic strain also calculated.

2.4. Plastic region type II

In this region, the stress values follow the condition $\sigma_\theta > \sigma_r > \sigma_z$, and the governing yielding state takes the form $\varphi = \sigma_\theta - \sigma_z = \sigma_0 r^{n_4}$. Here, based on the flow rule $\varepsilon_r^p = 0$, and from the incompressibility condition, $\varepsilon_\theta^P + \varepsilon_z^P = 0$ [19]. Therefore, $\varepsilon_\theta = \varepsilon_\theta^p + \varepsilon_\theta^e + \alpha T = -\varepsilon_z^p + \varepsilon_\theta^e + \alpha T$. Under the plane strain assumption leading to, $\varepsilon_z^p = -\varepsilon_z^e - \alpha T$, using this relationship and Eq. (3), we have:

$$\varepsilon_\theta = +\varepsilon_z^e + \varepsilon_\theta^e + 2\alpha T \tag{53}$$

By substituting the above relations into the strain compatibility equation, solving for stresses, and using equilibrium conditions, the governing differential equation for stresses in this regime derived as:

$$r^2 \frac{d^2\sigma_r}{dr^2} + p_1 r \frac{d\sigma_r}{dr} + P_2 \sigma_r = P_3 \omega^2 r^{n_5+2} + P_4 r^{n_4} + P_5 r^{n_1+n_2-n_3} + P_6 r^{n_1+n_2} \tag{54}$$

where;

$$P_1 = 3 - n_1 \tag{55}$$

$$P_2 = \frac{(1-2\nu)(1-2n_1)}{2(1-\nu)} \tag{56}$$

$$P_3 = -\frac{\left[(1-\nu)(n_5 - n_1 + 2) - 1\right]}{(1-\upsilon)}\rho_0 \tag{57}$$

$$P_4 = \frac{\left[(1-\upsilon)n_4 - n_1(1-\nu) + 1\right]}{2(1-\upsilon)}\sigma_0 \tag{58}$$

$$P_5 = \frac{-\alpha_0 E_0 D_1}{2(1+\nu)}\left[2(n_2 - n_3) + 1\right] \tag{59}$$

$$P_6 = \frac{-\alpha_0 E_0 D_2}{2(1-\nu)}\left[2(n_2) + 1\right] \tag{60}$$

The solution to the above differential equation is as follows:

$$\sigma_r(r) = C_5 r^{K_5} + C_6 r^{k_6} + q_1 \rho_0 w^2 r^{n_5+2} + q_2 \sigma_0 r^{n_4} + q_3 r^{n_1+n_2-n_3} + q_4 r^{n_1+n_2}) \tag{61}$$

Where:

$$K_{5,6}=\frac{-\left(P_1-1\right)^2\pm\sqrt{\left(P_1-1\right)^2-4p_2}}{2} \tag{62}$$

$$q_1=\frac{P_3}{\left(n_5+2\right)\left(n_5+1\right)+p_1\left(n_5+2\right)+P_2} \tag{63}$$

$$q_2=\frac{P_4}{n_4\left(n_4-1\right)+P_1n_4+P_2} \tag{64}$$

$$q_3=P_5/\left(\left(n_1+n_2-n_3\right)\left(n_1+n_2+n_3-1\right)+P_1\left(n_1+n_2-n_3\right)+P_2\right) \tag{65}$$

$$q_4=\frac{P_6}{\left(n_1+n_2\right)\left(n_1+n_2-1\right)+P_1\left(n_1+n_2\right)+P_2} \tag{66}$$

The tangential stress σ_θ is given by Eq. (1):

$$\sigma_\theta=C_5\left(K_5+1\right)r^{k_5}+C_6\left(K_6+1\right)r^{k_6}+q_1\left(n_5+n_4\right)\times\omega^2r^{n_5+2}+q_2\left(n_4+1\right)r^{n_4}+q_3\left(n_1+n_2-n_3+1\right)\times r^{n_1+n_2-n_3}+q_4\left(n_1+n_2+1\right)r^{n_1+n_2} \tag{67}$$

The axial stress based on the Tresca criterion is:

$$\sigma_z=\sigma_\theta-\sigma_0r^{n_4} \tag{68}$$

The tangential strain is $\varepsilon_\theta^{total}=\varepsilon_\theta^P+\varepsilon_\theta^e+\alpha T=\frac{u}{r}$ thus:

$$\varepsilon_\theta^P=\frac{1}{E\left(r\right)}(C_5\left(\left(K_5+1\right)\left(1-\nu\right)-\nu\right)r^{K_5}+C_6\left(\left(K_6+1\right)\times\left(1-\nu\right)-\nu\right)r^{K_6}+q_1\left(\left(n_5+4\right)\left(1-\nu\right)-\nu\right)\omega^2\times r^{n_5+2}+q_2\left(\left(n_4+1\right)\left(1-\nu\right)\right)r^{n_4}+q_3((n_1+n_2-n_3+1)\left(1-\nu\right)-\nu)r^{n_1+n_2-n_3}+q_4\left(\left(n_1+n_2+1\right)\times\left(1-\nu\right)-\nu\right)r^{n_1+n_2}+\alpha_0D_1r^{n_2-n_3}+\alpha_0D_2r^{n_2}-\sigma_0 \tag{69}$$

In this regime, $\varepsilon_r^P=0$, and $\varepsilon_\theta^P=-\varepsilon_z^P$.

2.5. Location of initiation and propagation of the plastic zone

The onset of yielding in a uniformly pressurized cylinder occurs at the inner radius [1]. In a functionally graded pressurized cylinder, however, yielding may initiate at the inner radius, the outer radius, simultaneously at both, or somewhere between the inner and outer surfaces. In contrast, for a rotating cylinder under a wide range of boundary conditions, yielding can initiate at the inner radius, the outer radius, or simultaneously at both locations [11].In the elastic state, Eqs. (23), (28), and (29) have expressed stress components. As the gradient parameters n_i, rotational speed ω, and temperature increase, both the stress values and the function φ increase until, for the first time φ reaches zero and this is the point at which yielding occurs.

2.5.1. Yield initiation at the inner radius (r=a)

By changing (and increasing) the values of ω and temperature, the stress levels continuously rise. With appropriate choices of the parameters n_i and temperature, yielding occurs at *r* =*a* at a critical angular velocity (denoted by ω_{e1}). In this case, the boundary conditions specified as follows:

$$\sigma_r^e\left(a\right)=-P_a \tag{70}$$

$$\sigma_r^e\left(b\right)=-P_b \tag{71}$$

Under these conditions, the plastic stress σ_i^p at *r*=*a* is equal to the elastic stress σ_i^e To determine the critical value ω_{e1}, Eqs. (70) and (71) are solved concurrently with the Tresca yield condition (expressed by Eq. (72)). From these

three equations, the constants C_1 and C_2 as well as ω_{e1} are determined in terms of the materials parameters and temperature.

$$\sigma_\theta^e(a) - \sigma_{min}^e(a) - \sigma_0 a^{n_4} = 0 \tag{72}$$

2.5.2. Yield initiation at the outer radius (r = b)

If, in Eq. (72), the inner radius *a* is replaced by the outer radius *b*, one obtains:

$$\sigma_\theta^e(b) - \sigma_{min}^e(b) - \sigma_0 b^{n_4} = 0 \tag{73}$$

By simultaneously solving Eqs. (70), (71), and (73), the critical angular velocity ω_{e2} is determined. The values of ω_{e1} and ω_{e2} are expressed as functions of the inner surface temperature T_a and the gradient parameters n_i, yielding families of curves corresponding to initiation at *r=a* or *r=b.*

2.5.3. Simultaneous yield initiation at the inner and outer radii

If Eqs. (70), (71), (72), and (73) solved simultaneously, the conditions under which yielding initiates from both surfaces obtained.

2.5.4. Propagation of the plastic zone

Following the onset of yielding (whether on the inner surface, outer surface, or both surfaces simultaneously), the plastic zone begins to expand with increasing load (due to higher rotational speed, elevated temperature, or increased n_i values). This expansion continues until the cylinder reaches full yielding. In the following section, we will numerically analyze this phenomenon.

3. Numerical results

To analyze the various mentioned cases, a MATLAB code developed to examine the resulting stresses under different conditions, including varying material property exponents, rotational speeds, and applied temperatures. Additionally, to enhance understanding and usability, the resulting diagrams plotted. For broader and more comprehensive results, the following dimensionless parameters used:

$$\bar{r} = \frac{r}{a}; \overline{\sigma_j} = \frac{\sigma_j(j=r,\theta,z)}{\sigma_0 a^{n_4}}; \Omega = \omega a\left(\frac{\rho_0 a^{n_5}}{\sigma_0 a^{n_4}}\right)^{0.5}; \overline{\varepsilon_j} = \frac{\varepsilon_j E_i}{\sigma_i}; \bar{u} = \frac{u E_i}{\sigma_i a} \tag{74}$$

$$\bar{\varphi}_1 = \left(\sigma_\theta - \sigma_r - \sigma_0 r^{n_4}\right) / \left(\sigma_0 a^{n_4}\right) \tag{75}$$

$$\bar{\varphi}_2 = \left(\sigma_\theta - \sigma_z - \sigma_0 r^{n_4}\right) / \left(\sigma_0 a^{n_4}\right) \tag{76}$$

Given the physical properties of FGM materials, the power-law exponents are defined as $n_1 = -2n_2 = -2n_3 = 2n_4 = n_5 = n$. In most analyses, the cylinder radius ratio *b/a*=1.5 Poisson's ratio *v*=0.3, yield stress $\sigma_0 = 250 Mpa/m^4$, and modulus of elasticity $E_0 = 2\times10^{11} Pa/m^4$ are assumed.

3.1. Elastic state

Using Eqs. (23) through (31), the dimensionless parameters, and the above conditions (with b/a=1.5), the elastic solution is derived. As the rotational speed increases from zero, the internal stresses in the cylinder grow. However, the radial stress distribution depends on the parameters n_i and T_a.

To illustrate and analyze the various stress components and dimensionless yield functions in the elastic region, Fig. 1 has been plotted. In Fig. 1, the radial, tangential, and axial stresses in the cylinder are depicted as functions of the radius for Ω=0.5 within the elastic region, the functions $\bar{\varphi}_1$ and $\bar{\varphi}_2$ are less than zero. However, given that the temperature in Fig. 1 exceeds zero degrees (T_a =400°), the radial stress is greater than the axial stress up to a radius of $\bar{r}=1.2901$ Beyond this radius, the axial stress exceeds the radial stress. By varying Ω across different values of n_i and T_a, a condition is reached where either $\bar{\varphi}_1$ or $\bar{\varphi}_2$ becomes zero. This indicates the point of yielding.

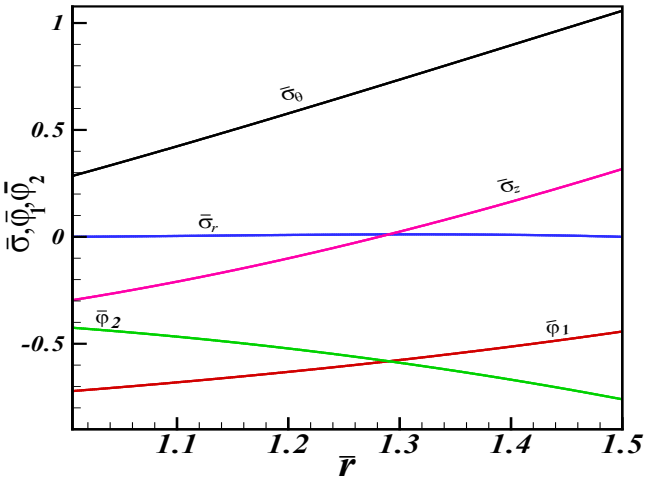

Fig. 1. Distribution of stresses and $\bar{\varphi}_1$ $\bar{\varphi}_2$ functions for angular speed ($\Omega=0.5$), temperature (T_a =400°) and $n=2$ in elastic regime

To observe the effect of increasing temperature on the yield functions, Fig. 2 has been plotted, showing the values of $\bar{\varphi}_1$ and $\bar{\varphi}_2$ for Ω=0.6869 and n=0.5 at temperatures of 0, 200, and 578 degrees.

As observed, at zero temperature, the value of $\bar{\varphi}_1$ throughout the cylinder exceeds that $\bar{\varphi}_2$, and its value becomes zero at the inner radius, indicating the onset of yielding at this point. The prevailing conditions at this stage correspond to Plastic Regime Type I. With an increase in T_a, the value $\bar{\varphi}_2$ continuously rises. Additionally, $\bar{\varphi}_1$ decreases near the inner radius and increases toward the outer radius. This change influences the governing yield conditions, meaning that, at constant Ω and n, and with an appropriate increase in temperature, the initiation of yielding at $r=a$ transitions from Plastic Regime Type I to Plastic Regime Type II.

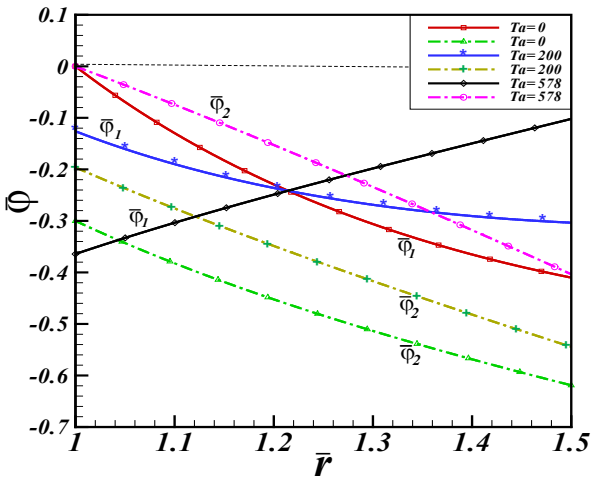

Fig. 2. Distribution of $\bar{\varphi}_1$ $\bar{\varphi}_2$ for angular speed (Ω = 0.6869), temperature (T_a =0°,200°,578°) and $n = 0.5$ at beginning of yielding

In other words, at the inner surface, as the temperature increases, $\bar{\varphi}_2$ approaches zero, and at 578°, it becomes zero. At this point, the inner radius is on the verge of yielding in the second plastic regime. Additionally, as the temperature increases, the outer surface gradually comes under the influence of the first plastic regime, approaching yield initiation.

3.2. Elastic-plastic state (yield initiation)

By simultaneously solving Eqs. (70), (71), and (72) for each temperature T_a and n, the value of Ω_{e1}, which leads to yield initiation at $r= a$, is determined. By considering $T_a = 200^\circ, 400^\circ$, b/a=1.5, -1<n<3 , these equations are solved, and the Ω_{e1} curve is derived. Additionally, by repeating this process and simultaneously solving the two boundary condition Eqs. (70) and (71) along with Eq. (73), the Ω_{e2} curve is obtained.

It should be noted that in each of Eqs. (72) and (73), two plastic regimes exist based on the minimum stress present in the equation, and depending on the conditions, one of these regimes may govern yielding. The resulting values of Ω_{e1} and Ω_{e2} are presented in Fig. 3.

As shown in Fig. 3(a), as Ω increases and reaches Ω_{e1} for example, with n=0.4 and Ω_{e1} =0.7302 the inner surface of the cylinder $\bar{r} = \bar{a}$ is on the verge of yielding, based on $\bar{\varphi}_1$. However, as the temperature increases for the same n, the yield threshold becomes Ω_{e1}=0.7317, which is determined by $\bar{\varphi}_2$. Therefore, the conditions governing yield initiation at the inner boundary depend on the temperature and may correspond to Plastic Regime Type I or II. However, for the outer surface, the governing yield regime is Plastic Regime Type I.

In Fig. 3, the Ω_{e1} and Ω_{e2} curves intersect at a critical point. For $T_a = 200$, this point corresponds to n_{cr} =1.5822 and Ω_{cr} =0.7158. For $T_a = 400^\circ$, it corresponds to n_{cr} =1.1001 and Ω_{cr} =0.7268. This critical point is obtained by simultaneously solving Eqs. (72) and (73) along with the boundary conditions.

According to Fig. 3, two regions are identified based on n_{cr} If $n < n_{cr}$ and Ω increases, the cylinder initially remains in the elastic region. Upon reaching out to Ω_{e1}, yielding occurs at r=a. As Ω increases further beyond this point, the plastic zone begins to expand, which falls outside the validity of the aforementioned equations.

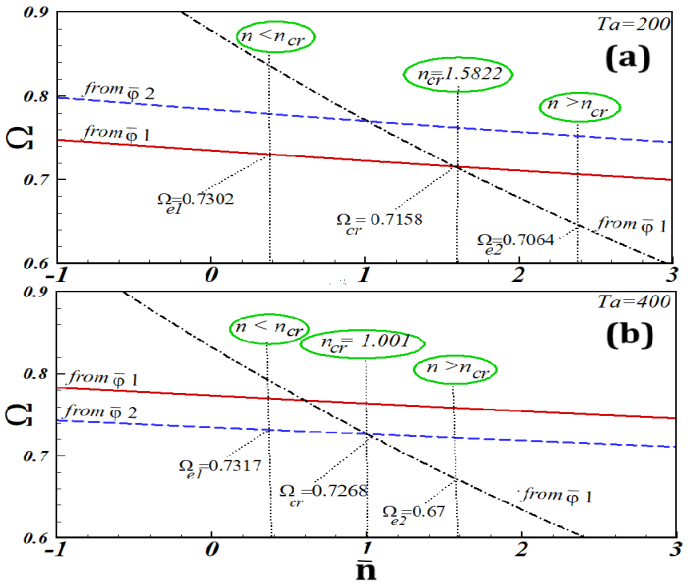

Fig. 3. Angular speeds for elastic limit $,\Omega_{e2},\Omega_{e1}$ versus "n" at temperatures (a) T_a =200°, (b) T_a =400°

Conversely, if $n > n_{cr}$, the cylinder initially remains in the elastic region until Ω reaches Ω_{e2}, leading to yielding at $r=b$. Increasing Ω beyond this point results in the plastic zone's growth. Therefore, the critical rotational speed governing yield initiation corresponds to the Ω_{e1} curve for $n < n_{cr}$ and the Ω_{e2} curve for $n > n_{cr}$.

For different temperatures Ta, the curves of Ω_{e1} and Ω_{e2} are plotted as functions of n in the range $-4<n<6$ in Figure 4. The intersection point of the two curves at each specific temperature represents the critical values n_{cr} and Ω_{cr} corresponding to that temperature.

The lower section of the obtained curves corresponds to the elastic region for each temperature, while the upper section represents the yielding threshold and plastic zone. As depicted in the figure, a series of graphs generated, delineating the elastic-plastic boundaries with respect to temperature, rotational speed, and material properties.

As the temperature increases up to approximately 312.5°, the value of n_{cr} decreases, while Ω_{cr} increases. For temperatures, exceeding 312.5°, n_{cr} continues to decrease but at a slower rate, and Ω_{cr} begins to decrease as well.

For temperatures below 312.5°, based on the elastic stress values obtained, the governing conditions for yield initiation are in the first plastic regime for both $n > n_{cr}$ and $n < n_{cr}$. However, for temperatures above 312.5°, the yield regime changes: for $n < n_{cr}$, the governing regime transitions to the second plastic regime, while $n > n_{cr}$, the first plastic regime continues to dominate.

If the properties of the functionally graded material remain constant ($n \geq n_{cr}^{0}$) and the temperature T_a is increased, yielding occurs at a lower Ω compared to the same material at zero temperature, initiating from the outer radius.

As the temperature rises, Ω_{e2} decreases for a fixed n. In the range $n_{cr}^{0} \leq n \leq n_{cr}^{700}$, moving leftward from the zero-temperature curve for a fixed n, increasing rotational speed initially leads to yielding at higher temperatures at the outer radius.

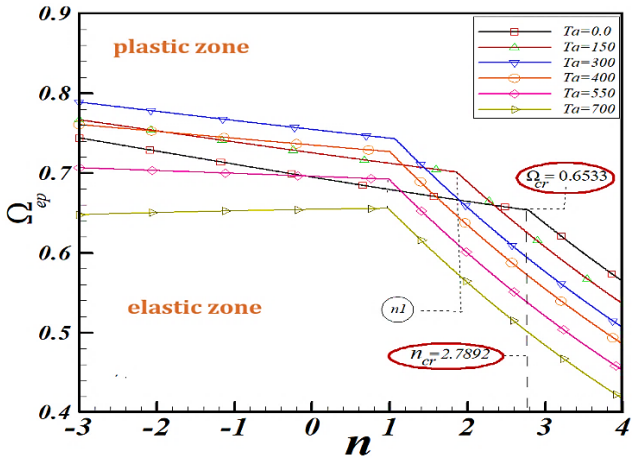

Fig. 4. Angular speed for elastic limits (Ω_{ep}) versus n for different temperature

Subsequently, as the rotational speed continues to increase, yielding occurs on curves corresponding to lower temperatures. For example, at n_1, with increased rotational speed, yielding initially occurs on the curve for T_a =700° at $\bar{b}$. As the rotational speed increases further, yielding occurs on curves corresponding to temperatures below 700°, until finally the cylinder is on the verge of yielding at $\bar{a}$ at zero temperature. Continuing to increase Ω leads to a critical point on the curve for T_a =150º.

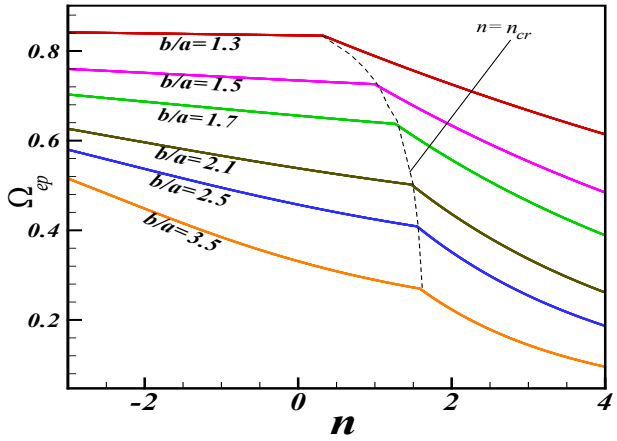

Fig. 5. Angular speed for elastic limit (Ω_{eq}) versus n at different radius ratio (b/a)

Another significant factor influencing the yield threshold of functionally graded cylinders, in addition to *Ta* and *n*, is the radius ratio of the cylinder. To examine this effect, the Ω_{ep} curves for different $\bar{b} = b/a$ ratios and *Ta*=200° are plotted in Fig. 5. By comparing the plotted curves, it can be observed that as b/a increases, n_{cr} rises. This increase ore pronounced for smaller radius ratios. However, the critical and limiting rotational speeds decrease with increasing b/a, effectively, the critical and limiting rotational speeds will significantly decrease.

Moreover, as the ratio of radii increases, the impact of material properties (*n*) on Ω_{eq} becomes more significant within the range of $n < n_{cr}$. To comprehensively analyze the influence of temperature and radius ratio $(\bar{b})$ on the critical rotational speed (Ω_{cr}) and critical index (n_{cr}), the corresponding curves are illustrated in Fig. 6 and Fig. 7. These plots examine the variations in critical values across different levels of the radius ratio ($\bar{b}$).

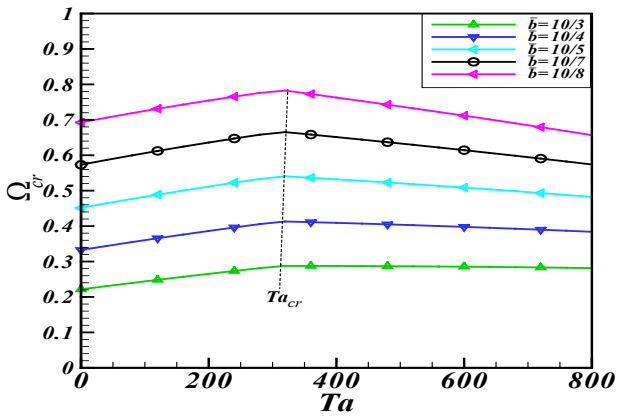

Fig. 6. Ω_{cr} curvs versus temperature at different radius ratio (b/a)

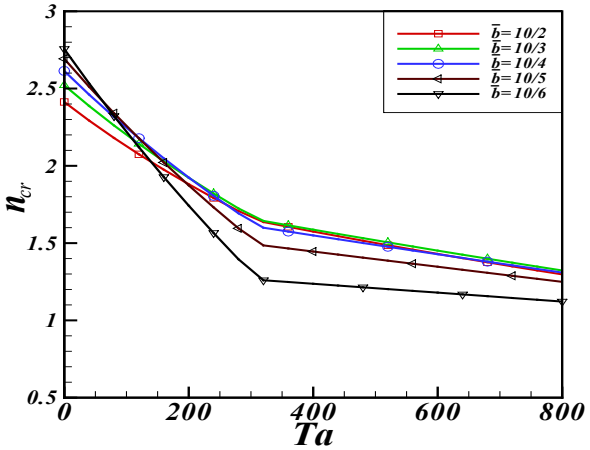

Fig. 7. n_{cr} curves versus temperature at different radius ratio (b/a)

According to Fig. 6, as the radius ratio decreases at a constant temperature, Ω_{cr} increases. The curves in the diagram reveal a maximum point on the Ω_{cr} curve. At this specific radius ratio, as the temperature rises, the critical rotational speed Ω_{cr} also increases, reaching a maximum at Ta_{cr} beyond this temperature, further increases lead to a decrease in the critical rotational speed. The critical temperature Ta_{cr}, for all $\bar{b}$ values lies within the range of 305 to 325 degrees. This behavior emphasizes the dependency of the critical rotational speed on both temperature and radius ratio in the system. According to Figure 7, as temperature increases, the value of n_{cr} decreases. The slope of the n_{cr} versus temperature curve differs before and after the critical temperature (Ta_{cr}). Prior to the critical temperature, n_{cr} declines more sharply with increasing temperature, while beyond the critical temperature, the rate of decrease in n_{cr} becomes more gradual. Across most temperature ranges, n_{cr} also decreases with reducing $\bar{b}$.

3.3. Plastic zone growth

If $\Omega = \Omega_{cr}$ and $n = n_{cr}$ the cylinder reaches the yield threshold at both $r = a$ and $r = b$. If Ω increases slightly, the cylinder enters the plastic zone, which begins to grow inward from b and outward from a.

In this case, two radii r_{ep1} and r_{ep2} are formed, which create three regions: the first region for $a \le r \le r_{ep1}$ the plastic region; the second region for $r_{ep1} \le r \le r_{ep2}$, the elastic region; and the third region for $r_{ep1} \le r \le b$, the plastic region.

In this case, the boundary conditions involve the continuity of stress and displacement at the borders of these regions, which can be expressed as follows:

$$\sigma_r^P(a) = -P_a = 0 \ , \ \sigma_r^P(b) = -P_b = 0 \qquad \sigma_r^P(r_{ep1}) = \sigma_r^e(r_{ep1}) \ , \ \sigma_r^P(r_{ep2}) = \sigma_r^e(r_{ep2})$$
$$\sigma_\theta^P(r_{ep1}) = \sigma_\theta^e(r_{ep1}) \ , \ \sigma_\theta^P(r_{ep2}) = \sigma_\theta^e(r_{ep2}) \quad u^p(r_{ep1}) = u^e(r_{ep1}) \ , \ u^p(r_{ep2}) = u^e(r_{ep2}) \tag{77}$$

By applying the boundary conditions from Eq. (77) and utilizing the equations for the elastic region ((23), (28), (29)) and plastic region, and solving them simultaneously, the unknowns C_1 ,C_2 *and* r_{ep1}, r_{ep2} can be determined for each Ω and *T*. Here, r_{ep1}, r_{ep2} represent the elastic-plastic radii within the cylinder.

As Ω gradually increases, the elastic-plastic radii expand, shrinking the elastic region until, at $\Omega_{fp} = \Omega$ and r_{ep1}, r_{ep2} coincide, resulting in the entire cylinder becoming plastic.

Fig. 8 depicts the growth of the plastic zone and the corresponding elastic-plastic radii for various temperatures up to 300 degrees. Up to this temperature, the plastic zones at the inner and outer surfaces are governed by the first plastic regime. At each temperature, the values of n_{cr} and Ω_{cr} ‹differ, leading to varying starting points for the plotted curves. The vertical values of each plot were offset by a constant numerical value to enable the simultaneous representation of all curves in a single figure with a common reference point. From the graphs in Fig. 8, it can observed that the growth of the plastic zone starts simultaneously on both sides.

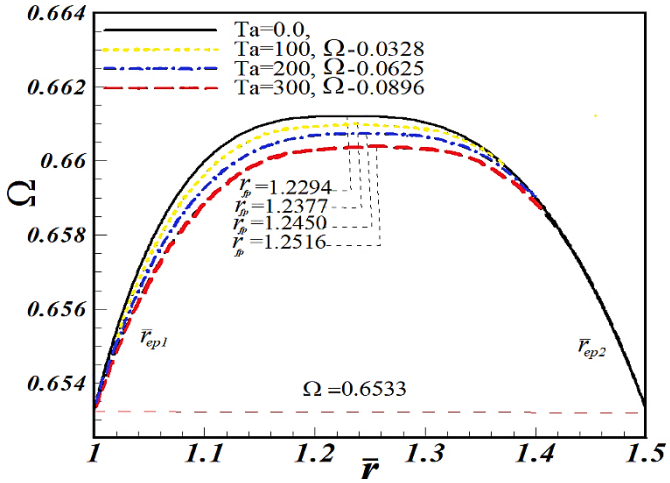

Fig. 8. Yield radii of the cylinder. (r_{ep2},r_{ep1}) in cylinder vesus angular speed at $\Omega \geq \Omega_{cr}$ *and* $n = n_{cr}$ for different temperature ($0^\circ \leq Ta \leq 300^\circ$)

However, the rate of growth from *a* and *b* depends on the temperature. At lower temperatures, the growth rate of the inner plastic zone is slower than that of the outer zone. Conversely, at higher temperatures, the growth rate of the inner plastic zone exceeds that of the outer zone (Fig. 8 and Fig. 9). Furthermore, with increasing temperature, the Ω range between the onset of the plastic zone and Ω_{fp} narrows, and the cylinder transitions into a fully plastic state with *a* smaller increase in rotational speed. If the operating temperature exceeds 312.5°, the dominant regime governing the growth of the plastic zone at the inner surface transitions to Plastic Regime Type II. As a result, the graphs differ from those in Fig. 8. For temperatures ranging from 400 to 800 degrees, and under conditions where $n = n_{cr}$ and $\Omega = \Omega_{cr}$, Fig. 9 illustrates the growth of the plastic zone.

According to Fig. 9, the growth of the plastic zone at the inner surface under Plastic Regime Type II is smaller than that at the outer surface under Plastic Regime Type I up to a temperature of 600°. However, at higher temperatures (700, 800 degrees), this trend is reversed.

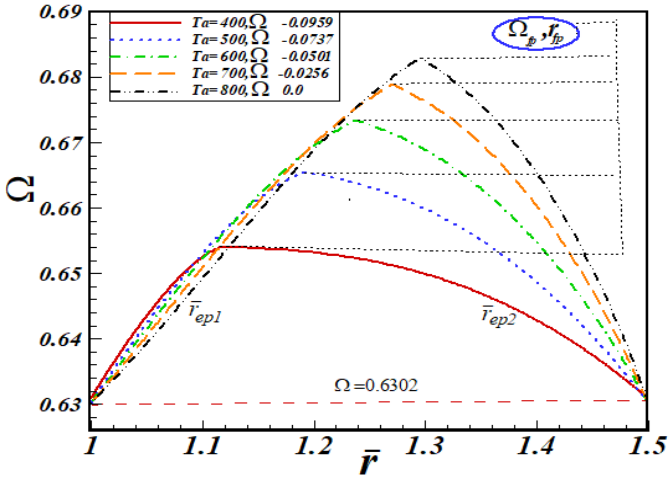

Fig. 9. Yielding bores (r_{ep2}, r_{ep1}) in cylinder versus angular speed at $\Omega \geq \Omega_{cr}$ *and* $n = n_{cr}$ for different temperature ($400^{\circ} \leq Ta \leq 800^{\circ}$)

With increasing temperature, the value of Ω_{cr} , for plastic initiation decreases, while Ω_{fp} increases. This implies that as the temperature rises, the rotational speed range between the onset and conclusion of the plastic zone expands. Additionally, under these conditions, for a given change in temperature, the variations in r_{fp} become more pronounced.

According to previous results, when $n > n_{cr}$, plastic yielding begins at $\Omega = \Omega_{e2}$ and at $r = b$ As Ω increases at a constant temperature, or as temperature increases at a constant Ω, the plastic zone grows.

Fig. 10 depicts this scenario, which is plotted for $n = 2.8 > n_{cr}$ and various temperatures. At n=2.8, for T_a=0, and Ω_{e2}=0.6525, plastic yielding begins at $r = b$, while a remains in the elastic region.

As Ω increases, the plastic zone grows from r=b, moving inward the cylinder's center. The boundary conditions in this case are as follows:

$$\sigma_r^P(a) = -P_a = 0 \;\; ; \;\; \sigma_r^P(b) = -P_b = 0 \; ; \sigma_r^P(r_{ep1}) = \sigma_r^e(r_{ep1}) \; ; \; \sigma_\theta^P(r_{ep1}) = \sigma_\theta^e(r_{ep1}) \; ; u^p(r_{ep1}) = u^e(r_{ep1}) \tag{78}$$

There are only two regions, an elastic for $a \leq r \leq r_{p1}$. and a plastic region for $r_{p1} \leq r \leq b$. As Ω increases, as shown in Fig. 10, yielding begins at a, and subsequently, with further increases in Ω, three regions similar to those in Fig. 8 emerge. This process continues until $\Omega = \Omega_{fp}$, where two plastic regions meet at $\bar{r}_{fp}$.

According to Fig. 10, as the temperature increases, the Ω value at which plastic deformation initiates at $\bar{b}$ decreases, whereas the Ω value at which yielding initiates at increases. If the temperature is sufficiently high (T_a >105°), during the expansion process of the plastic region, only two regions (elastic and plastic) will exist. Before the plastic region forms independently at $\bar{a}$, the expanding plastic region from $\bar{b}$ will reach $\bar{a}$

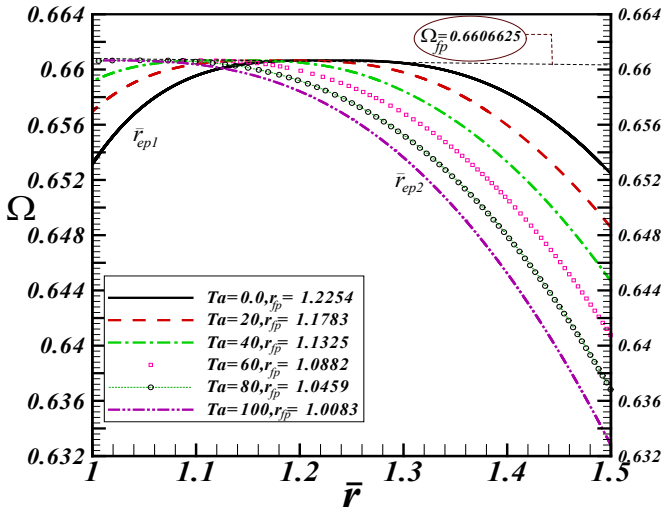

Fig. 10. Yielding bores (r_{ep2}, r_{ep1} .) in cylinder versus rotating speed at $n = 2.8 > n_{cr}$ for different temperature ($0^\circ \le Ta \le 100^\circ$.)

Based on the diagram, for n=2.8, the value of Ω_{fp} is identical across all temperatures studied, being Ω_{fp} =0.66066, and does not depend on the temperature (in the first type of plastic regime). Furthermore, the value of r_{fp} decreases with increasing temperature and becomes constant at *1* for T_a >105 degrees. If the above diagrams are plotted for higher $n > n_{cr}$, changes in r_{fp} relative to temperature become more significant, and $\bar{r}_{fp} = 1$ occurs at a lower temperature. If $n > n_{cr}$ is sufficiently larger, for instance, n=*4*, for $T_a > 0°$ and $\Omega \ge \Omega_{eq}$, only two regions (elastic and plastic) will form, and the plastic region formed at surface bb will grow inward until the cylinder becomes fully plastic at $r_{fp} = 1$.

Likewise, such analysis can be performed for $n < n_{cr}$ where. The onset of yielding starts from *a* and grows depending on temperature and *n*. To better illustrate the impact of temperature on the expansion of the formed regions, Fig. 11 has plotted. In this diagram, for four rotational speed values (Ω =0.6448, Ω =0.6552, Ω =0.6600, Ω =0.6606), the elastic-plastic radii and the yield front are plotted against temperature. According to the Fig. 11,in Ω =0.6448, as the temperature increases, the plastic region expands. The right side of the curve represents the plastic region, while the left side indicates the elastic region. At this rotational speed, with increasing temperature, there is no plastic region growth from $\bar{r} = \bar{a}$.

At Ω=*0.*6552, the boundary of the elastic-plastic region shifts to the left, and at T_a =*0*°, yielding occurs at the outer surface. With an increase in temperature, as shown in the figure, $\bar{r}_{ep}$ decreases.

By increasing the rotational speed to Ω=*0.*66, two plastic regions are observed, one growing from $\bar{b}$ and the other from $\bar{a}$. As the temperature increases from zero, both $\bar{r}_{ep1}$ and $\bar{r}_{ep2}$ decrease, meaning that at higher temperatures, the expansion of the plastic region from $\bar{b}$ toward $\bar{a}$ increases, while from $\bar{a}$ toward $\bar{b}$ it decreases. As Ω increases to Ω_{fp} , for all T_a values, only a single plastic region exists on both sides of $\bar{r}_{pp}$. Increasing the temperature shifts the location of r_{pp} , reducing its value until it approaches $\bar{r}_{pp} = 1$.

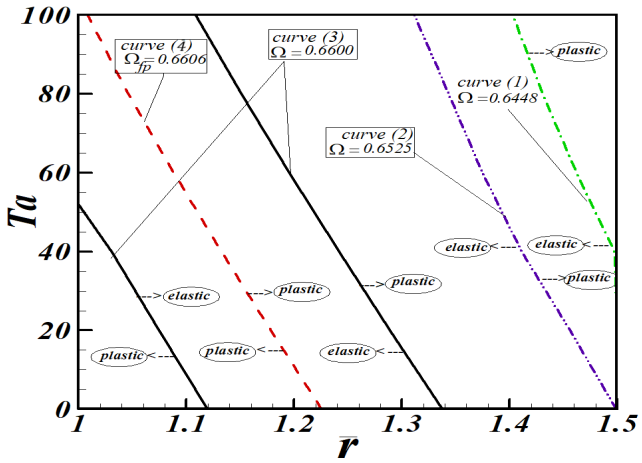

Fig. 11. Developing of plastic bores in cylinder versus temperature at $n = 2.8 > n_{cr}$ for $\Omega \le \Omega_{cr}$

4. Validation

To validate the present work, the values of n_2, n_3, n_4, n_5, were set to zero, and the graph of plastic region growth for T_a =0° and n=1.5 was plotted. in Fig. 12(a) The results were compared with those presented in [10]. For plotting this graph, the stated conditions and the dimensionless equations from the reference were utilized. As evident in Fig. 12(a), the responses are in complete agreement. Moreover, considering the reference conditions from [17], including internal pressure ($Pa=60\,MPa$), T=0° n_2 *and* n_3 equal to zero, the plastic region growth in the cylinder for $n_{cr} = 3.729$ and $\Omega \ge \Omega_{cr}$ was plotted in Fig. 12(b). Full agreement observed between the values of this study and reference [17].

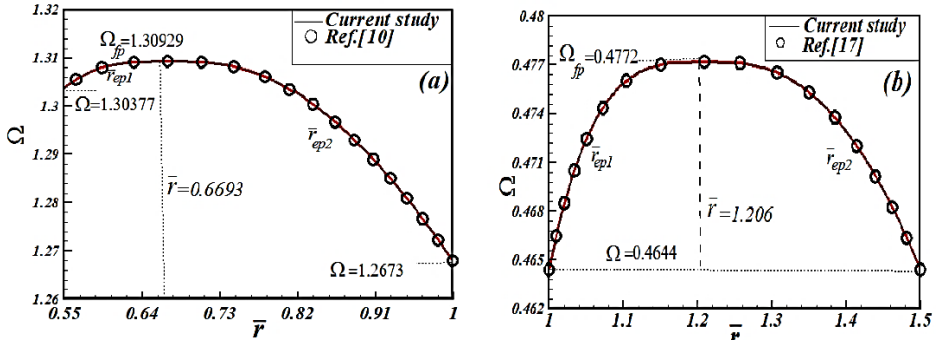

Fig. 12. validation of current study at zero temperature with (*a*) [10] and (*b*) [17] references

5. Conclusion

This study investigated the impact of thermal loads, material composition, and rotational speed on the initiation and expansion of the plastic region in a functionally graded rotating cylinder. In the rotating cylinder, within the elastic region, the yield functions are less than zero. With the increase in rotational speed or temperature, these functions reach zero, marking the onset of yielding. It was demonstrated that, in the presence of thermal loads, two plastic regimes based on the Tresca criterion ($\bar{\varphi}_1$ and $\bar{\varphi}_2$) are required to explain the elastic-plastic solution. Accordingly, the onset of yielding depends on the values of Ω, n_i, and T_a, and may occur at the inner surface, the outer surface, or simultaneously at both surfaces. However, for homogeneous materials ($n_i = 0$), yielding begins at the inner surface

at various temperatures, although the required rotational speed threshold for initiating yielding differs. Additionally, it shown that an increase in temperature significantly affects stress values and, consequently, the plastic regime. If the temperature is zero or below a critical value, the governing plastic regime is the first type. At temperatures above the critical threshold, the governing regime is the second type for the inner surface and the first type for the outer surface. The plastic limit speeds are also affected by temperature, such that, with constant n at $r=b$ or $r=a$ and for $Ta \geq Ta_{cr}$ an increase in temperature leads to yielding initiation at a lower Ω If $Ta \leq Ta_{cr}$, an increase in temperature raises the Ω required for yielding initiation. Additionally, the value of Ω_{cr} increases with temperature but decreases at temperatures higher than the critical temperature. Regarding n_{cr}, it can be observed that its value decreases with increasing temperature; however, after the critical temperature, the rate of decrease becomes minimal, and n_{cr} stabilizes within a limited range.

In the next phase, the growth of the plastic region was examined. In the case where $n=n_{cr}$ and $\Omega \geq \Omega_{cr}$, two plastic regions grow from the boundaries of a and b inward into the cylinder, resulting in three regions "plastic-elastic-plastic". As Ω increases, the size of the elastic region decreases until, at $\Omega = \Omega_{fp}$ and $r = r_{fp}$, the two plastic regions meet. The increase in temperature from zero to the critical temperature, at constant n_{cr}, reduces the range of $\Omega_{ep} < \Omega < \Omega_{fp}$. however, for $Ta \geq Ta_{cr}$, it increases the range. Beyond the critical temperature, this range and the radius of full plastic deformation increase. If n is constant and slightly greater than n_{cr}, yielding initiation and growth begin at the surface b, initially forming only two regions elastic and plastic. With increasing Ω, yielding also initiates from the inner surface and expands until the two plastic regions meet at r_{pp}.

Temperature increase reduces the rotational speed required for plastic initiation at b while increasing it at a. If the temperature increase is sufficient, the front of the plastic region expanding from b reaches a before yielding occurs at a. If n is constant and slightly less than n_{cr}, similar results are obtained, with yielding initiation starting from a.

The size ratio b/a significantly affects Ω_{cr}, n_{cr} and the values of Ω_{e1} and Ω_{e2}. It can be concluded that, with an increase in the radius ratio at constant temperature, the rotational speed required for plastic initiation decreases, and the cylinder yields at a lower rotational speed. However, the value of n_{cr} increases with the radius ratio at constant temperature, and overall, the variations in Ω_{cr} due to changes in material properties are more pronounced at higher radius ratios.

Temperature changes also have a considerable impact on Ω_{cr} and n_{cr} for different radius ratios. With a decrease in b/a, n_{cr} decreases; however, Ω_{cr} increases up to a certain temperature, which depends on the geometry and conditions of the problem (approximately 305 to 325 degrees in this case), and then decreases.

References

[1] Gamer, U., Lance, R. H., 1983. Stress distribution in a rotating elastic-plastic tube. Acta Mechanica, 50(1), 1-8. https://doi.org/10.1007/BF01170437

[2] W. Mack., 1991. Rotating elastic–plastic tube with free ends, International journal of Solids and Structure, vol. 27, pp 1461–1476. https://doi.org/10.1016/0020-7683(91)90042-E

[3] Eraslan, A. N., 2003. On the linearly hardening rotating solid shaft. European Journal of Mechanics - A/Solids, 22(2), 295-307. https://doi.org/10.1016/S0997-7538(02)00002-5

[4] Eraslan, A. N., 2004. Von mises' yield criterion and nonlinearly hardening rotating shafts. Acta Mechanica, 168(3), 129-144. https://doi.org/10.1007/s00707-004-0088-z
[5] Eraslan, A. N., Mack, W., 2005. A computational procedure for estimating residual stresses and secondary plastic flow limits in nonlinearly strain hardening rotating shafts. Forschung im Ingenieurwesen, 69(2), 65-75. https://doi.org/10.1007/s10010-004-0138-7
[6] Eraslan, A. N., Akis, T., 2005. Elastoplastic Response of a Long Functionally Graded Tube Subjected to Internal Pressure. Turkish Journal of Engineering & Environmental Sciences, 29(6).
[7] Eraslan, A. N., Akis, T., 2006. On the plane strain and plane stress solutions of functionally graded rotating solid shaft and solid disk problems. Acta Mechanica, 181(1), 43-63. https://doi.org/10.1007/s00707-005-0276-5
[8] Eraslan, A. N., Akis, T., 2006. Plane strain analytical solutions for a functionally graded elastic–plastic pressurized tube. International Journal of Pressure Vessels and Piping, 83(9), 635-644. https://doi.org/10.1016/j.ijpvp.2006.07.003
[9] Eraslan, A. N., Akis, T., 2006. The stress response of partially plastic rotating fgm hollow shafts: Analytical treatment for axially constrained ends. Mechanics Based Design of Structures and Machines, 34(3), 241-260. https://doi.org/10.1080/15397730600779285
[10] Akis, T., Eraslan, A. N., 2007. Exact solution of rotating fgm shaft problem in the elastoplastic state of stress. Archive of Applied Mechanics, 77(10), 745-765. https://doi.org/10.1007/s00419-007-0123-3
[11] Eraslan, A. N., Arslan, E., Mack, W., 2007. The strain hardening rotating hollow shaft subject to a positive temperature gradient. Acta Mechanica, 194(1), 191-211. https://doi.org/10.1007/s00707-007-0456-6
[12] Darijani, H., Kargarnovin, M. H., Naghdabadi, R., 2009. Design of thick-walled cylindrical vessels under internal pressure based on elasto-plastic approach. Materials & Design, 30(9), 3537-3544. https://doi.org/10.1016/j.matdes.2009.03.010
[13] Ozturk, A., Gulgec, M., 2011. Elastic–plastic stress analysis in a long functionally graded solid cylinder with fixed ends subjected to uniform heat generation. International Journal of Engineering Science, 49(10), 1047-1061. https://doi.org/10.1016/j.ijengsci.2011.06.001
[14] Pankaj, T., 2011. Elastic-plastic transition stresses in rotating cylinder by finite deformation under steady-state temperature. Thermal Science, 15(2), 537. https://doi.org/10.2298/TSCI090715041P
[15] Sharma, S., Yadav, S., 2013. Thermo elastic-plastic analysis of rotating functionally graded stainless steel composite cylinder under internal and external pressure using finite difference method. Advances in Materials Science and Engineering, 2013(1), 810508. https://doi.org/10.1155/2013/810508
[16] Fatehi, P, Nejad, M. Z., 2014. Effects of material gradients on onset of yield in fgm rotating thick cylindrical shells. International Journal of Applied Mechanics, 06(04), 1450038. https://doi.org/10.1142/S1758825114500380
[17] Nejad, M. Z, Fatehi, P., 2015. Exact elasto-plastic analysis of rotating thick-walled cylindrical pressure vessels made of functionally graded materials. International Journal of Engineering Science, 86, 26-43. https://doi.org/10.1016/j.ijengsci.2014.10.002
[18] Timoshenko, S. P., Goodier, J. N., 1970. Theory of Elasticity, New York: McGraw-Hill.
19] Mendelson, A., 1968. Plasticity: Theory and Application, New York: Macmillan.